Aerodynamic design of the wing-fuselage junction for the high-performance sailplane Mü-31

Rolf Berger, L.M.M. Boermans

Akaflieg München, TU-München, Germany
Faculty of Aerospace Engineering, Delft University of Technology, The Netherlands

Presented at the XXVII OSTIV Congress in Leszno, Poland

Introduction

An analysis and design process is described for a new wing-fuselage junction to be applied in the high-performance sailplane Mü-31 of Akaflieg München, Figure 1. First, wind-tunnel geometries that were previously tested are analysed with a panel code. The mathematical background is described, which enables the interpretation and understanding of the unexpected experimental data. The new design is developed on the basis of one of the previous wind-tunnel geometries, taking construction guidelines and limitations into account. The wing center section and the fuselage are changed iteratively to improve the configuration in potential flow first, i.e. with respect to induced drag. The integral design process is extended with viscous calculations to identify transition and areas prone to separation.

The Mü-31 is a sailplane prototype aiming at an improved wing-fuselage design described in the present work. With a wingspan of 15 meters and camber-changing flaps, the Mü-31 fulfils all requirements of the FAI 15-Meter Class that is flown at all major championships. To reduce costs and time, existing moulds of the ASW-27 - manufactured by Alexander Schleicher Segelflugzeugbau GmbH in Germany - will be used for the cockpit, the outer wings and the stabilizers. The center section of the wing and the fuselage contain the new approach in wing fuselage design.

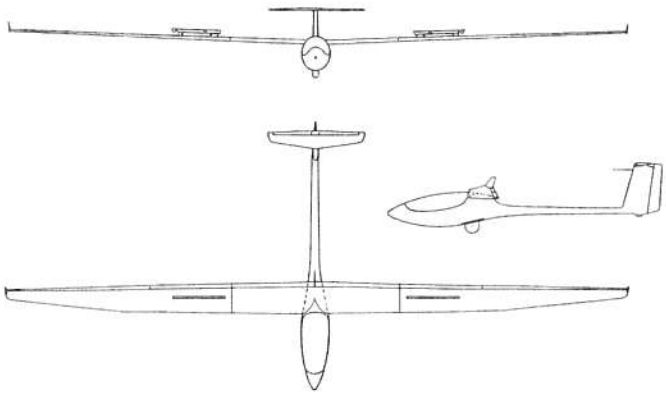

Figure 1. Drawing of the Mü-31 sailplane.

Flow phenomena

The wing-fuselage interference effects of high-performance sailplanes can be distinguished between inviscid- and viscous effects (ref.1):

Inviscid effects

In a wing-fuselage combination, the fuselage is capable of carrying over circulation depending on the arrangement and shape of the fuselage with respect to the wing. In the proximity of the fuselage the nearly elliptical circulation distribution of the wing is

disturbed, increasing the induced drag (ref. 2). Classical theory shows that this increase is only 0.5% in the ideal case for a midwing 15-meter span sailplane (ref. 8), and hence, it is usually ignored.

More important is the so-called "alpha-flow"-effect, which describes the mutual influence of the wing and fuselage in dependence of the angle of attack, Figure 2. The circulation of the wing is responsible for an upward flow in front of the wing. At positive angles of attack, the additional upflow due to crossflow of the fuselage increases the flow angle towards the wing root. At negative angles of attack, this flow angle is reduced.

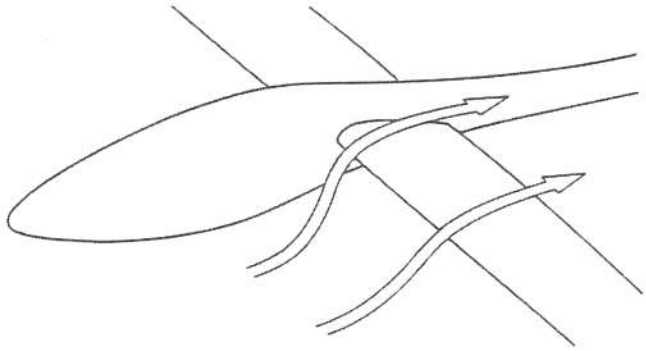

Figure 2. Alpha-flow effect (ref. 1).

Viscous effects

Due to the contraction of the fuselage and the stagnation point on the wing root, an adverse pressure gradient exists on the fuselage in front of the wing, which causes the laminar boundary layer to turn turbulent in front of the wing, Figure 3. The turbulent boundary layer cannot cope with the steep pressure gradient either and separates, forming a system of horseshoe vortices that fold around the wing root and extend downstream on the fuselage. On the wing, at low angles of attack, a turbulent wedge occurs on the lower and upper surface that originates at the wing root leading edge. At higher angles of attack, due to the alpha-flow effect, transition on the upper surface moves forward towards the wing root. On the lower surface this occurs at negative angles of attack.

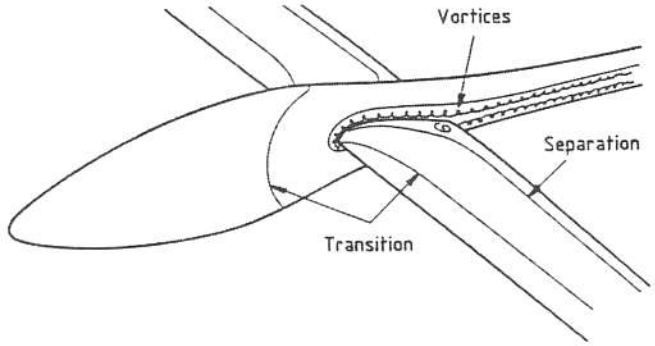

Figure 3. Viscous flow effects (ref. 1).

To reduce the wetted surface of a high-performance sailplane, the fuselage is contracted in the region of the wing-fuselage junction. The contraction of the fuselage leads to an adverse pressure gradient that adds to the adverse gradient of the wing root. Hence, at the juncture towards the trailing edge, the flow over the wing is prone to separation (refs. 1 and 3).

Basic concept

Windtunnel analysis

The analysis is based on wind-tunnel experiments (ref. 4), which were carried out in 1997 in the Low Speed Low Turbulence Windtunnel of Delft University of Technology, Faculty of Aerospace Engineering. In this experiment a new wing-fuselage concept was investigated. The experiment was repeated in 2002 (ref. 5) because the differences in drag of the windtunnel models were unexpectedly large.

Three 1:5 scale models that differed in their wing-fuselage geometry were subject to this research; the models are shown in Figure 4 and Figure 5.

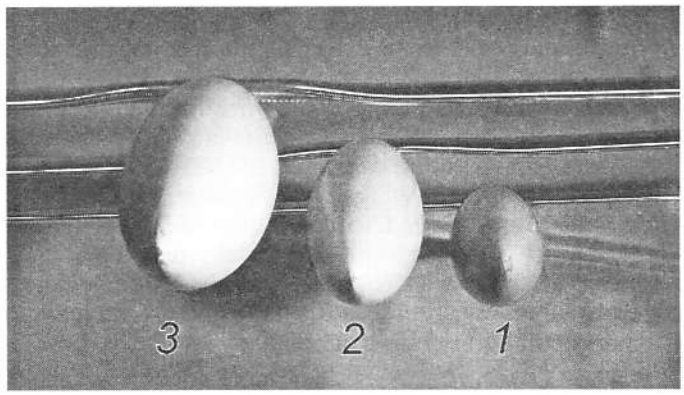

Figure 4. Windtunnel models No. 1, 2 and 3.

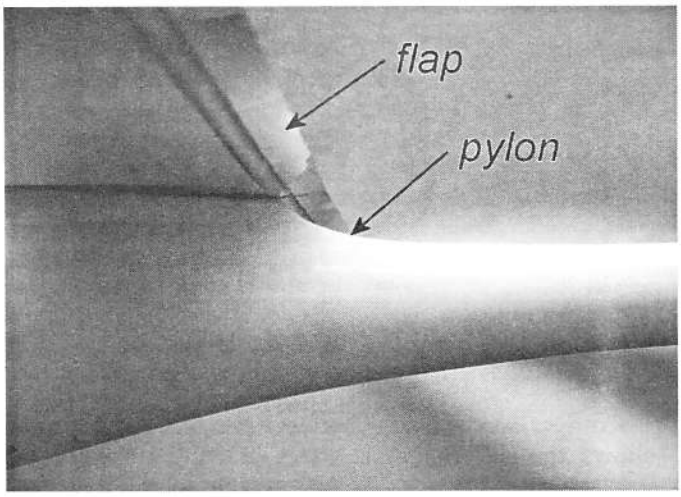

Figure 5. High-wing-pylon configuration.

The main goal of this new geometry was the realization of a high-wing configuration that has several benefits. Since the upper wing surface of the high-wing configuration is washed by less boundary layer flow coming from the fuselage, the start of boundary layer separation is expected to be delayed, allowing for better

low-speed flight capabilities than conventional midwing configurations. Another feature is the contraction of the fuselage below the wing, leading to a reduced wetted surface of the tailcone. In midwing configurations the horseshoe-vortices at the wing root affect the tailcone of the sailplane. The present pylon-like wing configuration, Figure 5, is expected to reduce the influence on the rear fuselage as the vortices leaving the pylon do not touch the fuselage.

Model 1 is the basic geometry with a constant chord wing that spans the tunnel width. The laminar airfoil DU89-134/14 (ref. 6) extends along the whole wingspan. As this research was focused on the wing-fuselage interference, the models had no tailplanes. For model 2, a positive twist is applied to the wing in the vicinity of the fuselage. And finally, model 3 has the same twisted wing as model 2, plus a special wing-root airfoil suited for a turbulent boundary layer. The wing twist is applied by rotation around the flap hinge axis to allow for a continuous flap. Descriptions of the models are given in ref. 7.

The wing was suspended by a pivot through the windtunnel walls to an external frame connected to the windtunnel balance system, as described in ref. 8. The measurements were carried out first for the wing only using both the balance system and a wake rake traversing in spanwise direction, the difference being the drag resulting from wingtip-wall interference. Standard methods were applied to correct for blockage and lift interference. All configurations were tested at a flap setting of 0° and 20°. The Reynolds Number for all experiments was 700,000. Figure 6 shows the experimental lift versus drag data.

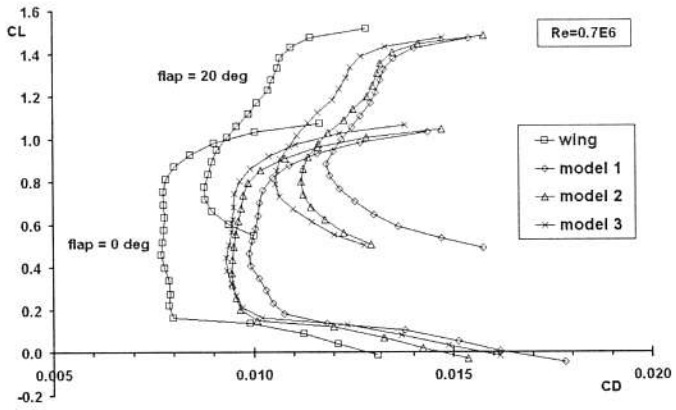

Figure 6. Exp. data, Re = 7E5, flap 0° and 20° (ref. 5).

Comparison of results between models 1 and 2 clearly shows the advantageous effect of wing twist for both flap settings. The drag reduction from model 2 to model 3 was achieved with a "turbulent friendly" wing root section. Within the turbulent wedge a turbulent airfoil is superior to a laminar airfoil, since it is able to cope with turbulent flow without separation. Remarkably, the drag reduction due to twist and wing root modification applied to model 3 is about 30% of the drag difference between model 1 and the wing only.

Computational analysis

To clarify the experimental data, a computational analysis was carried out. Since inviscid- as well as viscous effects were of interest, a coupled panel- and boundary layer method was chosen. The commercial panel-code VSAero, version 6.2, satisfied the requirements (ref. 9, 10).

In order to investigate the circulation distribution and induced drag, the inviscid- (potential) and incompressible Trefftz Plane Analysis was used. With this far field analysis, the lift and the induced drag are calculated in a plane behind the body. The wake shed from the body contains all the information necessary to compute the lift and induced drag.

Mathematical background

The induced drag coefficient in the Trefftz Plane behind a planar wing is:

$$C_{Di} = \frac{2}{U_\infty^2 \cdot S} \int_{-b/2}^{b/2} \Gamma(y) \cdot w_i(y) \cdot dy \qquad (1.1)$$

and the lift coefficient is:

$$C_L = \frac{2}{U_\infty \cdot S} \int_{-b/2}^{b/2} \Gamma(y) \cdot dy \qquad (1.2)$$

At the trailing edge of the wing a wake is shed - in the present case not interrupted by the fuselage - that contains the circulation $\Gamma(y)$ and the induced downwash $w_i(y)$. Using a discrete number of wake panels, the integrations become summations over n:

$$C_{Di} = \frac{2}{U_\infty^2 \cdot S} \sum_n \Gamma_n \cdot w_{i_n} \cdot \Delta y_n \qquad (1.3)$$

$$C_L = \frac{2}{U_\infty \cdot S} \sum_n \Gamma_n \cdot \Delta y_n \qquad (1.4)$$

In the equation for the induced drag (Eq. 1.1, 1.3), the circulation and the induced downwash of an arbitrary wing with twist at angle of attack α can be split into two terms (ref. 2):

$$\Gamma(y) = \alpha \cdot \Gamma_u(y) + \Gamma_0(y) \qquad (1.5)$$

$$w_i(y) = \alpha \cdot w_{iu}(y) + w_{i0}(y) \qquad (1.6)$$

In both equations, the first term on the right hand side belongs to the untwisted wing (index "u"), while the second terms represent the twisted wing at zero-lift (index 0), being the zero-lift circulation $\Gamma_0(y)$ and the zero-lift downwash $w_{i0}(y)$. Eq. (1.5) demonstrates that the circulation of a twisted wing can be calculated by superimposing the circulation of the untwisted wing with the zero-lift circulation of the twisted wing.

Figure 7 shows the circulation distributions of a twisted wing. Due to the negative twist in the inner wing, the inner wing is generating a negative- and the outer wing a positive- lift force as shown in the circulation distribution for zero lift $\Gamma_0(y)$. At a non-zero angle of attack, an elliptical circulation $\alpha(y) \cdot \Gamma_u(y)$ is added to the zero-lift circulation $\Gamma_0(y)$. It is obvious that the detrimental effect of the zero-lift circulation relatively weakens at higher angles of attack.

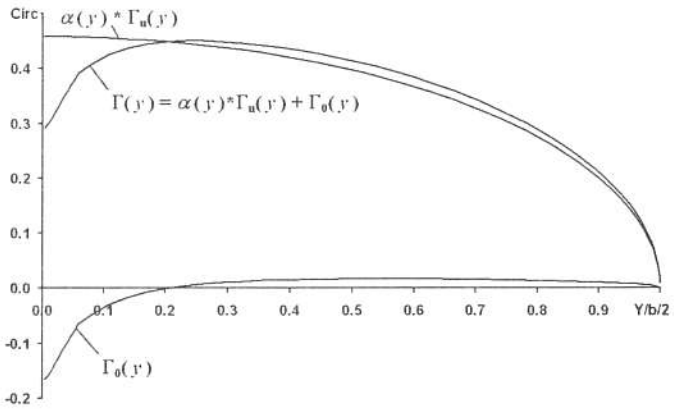

Figure 7. Superposition of circulation.

Using Eqs. (1.5) and (1.6), the induced drag coefficient in Eq. (1.1) can be written as:

$$C_{Di} = \frac{2}{U_\infty^2 \cdot S}\int_{-b/2}^{b/2}\alpha^2 \cdot \Gamma_u \cdot w_{iu}\cdot dy + \frac{2}{U_\infty^2 \cdot S}\int_{-b/2}^{b/2}\alpha \cdot \Gamma_u \cdot w_{i0}\cdot dy + \frac{2}{U_\infty^2 \cdot S}\int_{-b/2}^{b/2}\alpha \cdot \Gamma_0 \cdot w_{iu}\cdot dy + \frac{2}{U_\infty^2 \cdot S}\int_{-b/2}^{b/2}\Gamma_0 \cdot w_{i0}\cdot dy \qquad (1.7)$$

Using

$$\alpha = \frac{C_L}{C_{L\alpha}} \qquad (1.8)$$

this equation can be written as:

$$C_{Di} = C_2\frac{C_L^2}{\pi \cdot A} + C_1 C_L + C_0 \qquad (1.9)$$

where A is the aspect ratio of the wing. The factors C_0, C_1 and C_2 are:

$$C_0 = \frac{2}{U_\infty^2 S}\int_{-b/2}^{b/2}\Gamma_0 w_{i0}\,dy \qquad (1.10a)$$

$$C_1 = \frac{2}{U_\infty^2 S C_{L\alpha}}\int_{-b/2}^{b/2}(\Gamma_u w_{i0} + \Gamma_0 w_{iu})\,dy \qquad (1.10b)$$

$$C_2 = \frac{2\cdot\pi\cdot A}{U_\infty^2 S C_{L\alpha}^2}\int_{-b/2}^{b/2}\Gamma_u w_{iu}\,dy \qquad (1.10c)$$

For an untwisted wing the factors C_0 and C_1 are zero and with C_2=k, Eq. (1.10) reduces to

$$C_{Di} = k \cdot \frac{C_L^2}{\pi \cdot A} \qquad (1.11)$$

This well known relation between lift and induced drag is often also used for twisted configurations. In that case, the k-factor is a function of C_L and not only a factor describing the efficiency of the wing-planform. Summarizing all effects in one coefficient k is convenient when the aerodynamic efficiency of arbitrary configurations is compared. It should be realized, however, that the induced drag at zero lift coefficient is not necessarily zero, as suggested by Eq. (1.11). C_0 only comes into existence for a twisted wing. It corresponds to the induced drag at zero lift. Finally, C_1 is a factor that combines the twisted and untwisted circulations; for nearly elliptical circulation distributions, C_1 is negligibly small.

The effect of the fuselage, as reflected in the circulation distribution in the Trefftz Plane, is similar to twist in the wing center section, as will be shown.

Results

For all wing-fuselage configurations, the circulation distribution obtained from the Trefftz Plane Analysis was compared to the circulation distribution of the untwisted wing without fuselage. The wing had the same twist as applied in wind-tunnel models 1 and 3. The results of the Trefftz Plane Analysis are presented in Figure 8 for wings with the twist applied in model 1 and model 3 and for the untwisted wing without fuselage, at lift coefficients of C_L=0.3 and C_L=1.2 and flap deflections of 0° and 20° respectively.

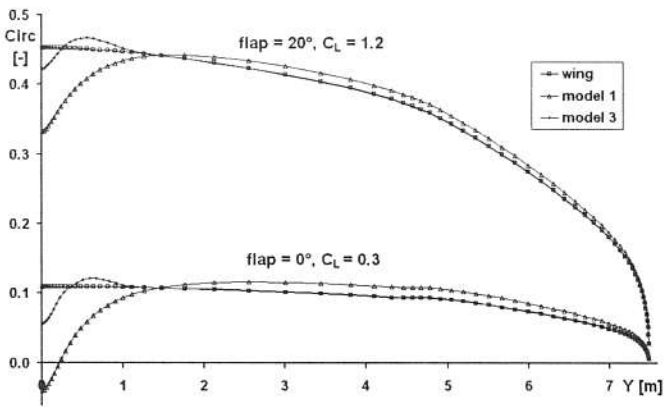

Figure 8. Circ. distr. at C_L=0.3 and 0° flap deflection Circ. distr. at C_L=1.2 and 20° flap deflection.

Figure 8 shows that the circulation of the wing without twist, as in the case of model 1, is strongly influenced by the presence of the fuselage. From 0 to 1 meter wingspan, an especially large loss of circulation was calculated, even dropping to negative values in the centre section of the wing at C_L=0.3. At the same lift coefficient as the untwisted wing, the wing beyond 1.5 meter span of model 1 has to generate more circulation

to compensate for the loss of circulation in the centre section.

The analysis of the twisted wing of model 3 indicates an improvement of the circulation distribution compared to the untwisted case. Remarkably, the twist is compensating in the first meter of wingspan, leaving the rest of the wing unaffected. But the twist is not ideal and there is still an unfavourable circulation distribution between 0 and 1 meter wingspan.

Similar to the case of twist, the disadvantageous effect of the fuselage is relatively weaker at higher lift coefficients.

The lift coefficient C_L and the induced drag coefficient C_{Di} are calculated with Eqs. (1.3) and (1.4). The k-factor is derived for each configuration with Eq. (1.11) and A=25, S=9m², and plotted as a function of the lift coefficient in Figure 9.

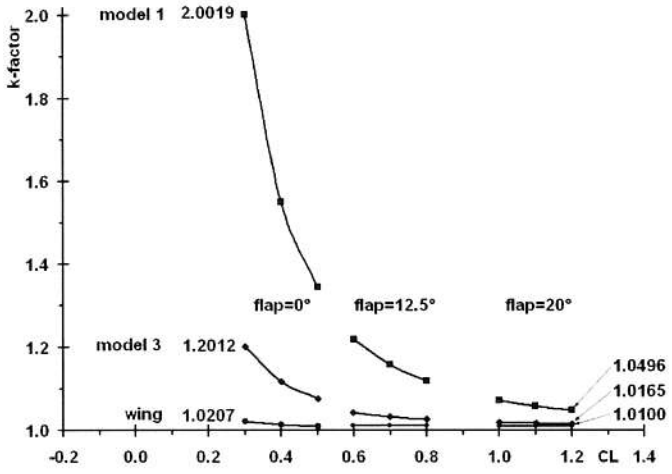

Figure 9. k-factors: model 1, model 3 and wing.

For the wing only, the k-factor is varying from k=1.0207 at C_L=0.3 to k=1.01 at C_L=1.2. A k-factor of k=1.01 for this particular planform was also determined with a lifting line method in ref. 12.

The results for the case without twist (model 1) show the large detrimental effect of the presence of the fuselage on the circulation distribution over the whole C_L-range. At large lift coefficients, the performance is about 4% worse, compared to the wing only case. This loss increases for smaller lift coefficients down to C_L=0.3 where the induced drag is about 100% larger than the wing only case.

The wing twist applied in model 3 reduces the induced drag appreciably. At C_L=0.3 the k-factor drops from k=2.0019 (model 1) to k=1.2012 (model 3), but is still 18% worse than the wing only case. At larger lift coefficients, this configuration improves gradually, nearly reaching the k-factor of the wing only at C_L=1.2.

With these general results, the windtunnel experiments can be explained qualitatively. In Figure 10, both the experimental data (Figure 6) and the calculated results are presented.

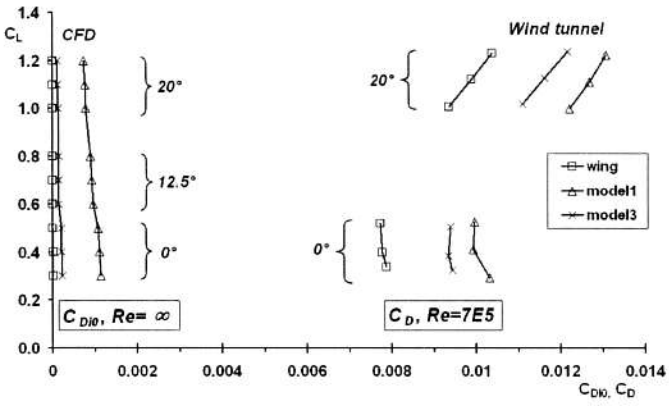

Figure 10. Windtunnel results and CFD-results.

The experimental data, referred to a standard wing area of 10m², are plotted on the right hand side of the graph. The total drags of model 1 and model 3 are composed of the drag of the wing (which extends from wall to wall to simulate an infinite span with zero induced drag), the fuselage, and the mutual interference. For comparison, earlier tests with eight wing-fuselage combinations indicated a fuselage drag contribution of about 0.001 (ref. 8). The interference drag has viscous and inviscid components; the latter is the induced drag due to the presence of twist and the fuselage (Eq. 1.10a). A flap setting of 12.5° was not tested.

The inviscid drag resulting from the CFD analysis, referred to 9m² wing area, are plotted on the left side. The induced drag of the untwisted wing is subtracted, leaving the induced drag due to twist (model 3) and the presence of the fuselage, to allow for a comparison with the experiment. The drag of the wing, fuselage and interference have not been added to the CFD results in order to reproduce the windtunnel data, because these contributions are not yet theoretically predictable with the required accuracy. In a qualitative comparison, however, it is evident that the change in induced drag due to twist and presence of the fuselage is responsible for the almost parallel shift of the windtunnel data.

Figures 11 and 12 present the three-dimensional pressure distributions on model 1 and 3 at C_L=0.3 and a flap deflection of 0°. The low pressures on the lower side of the wing indicate the cause of the lift loss, especially in the case of model 1. The wing twist of model 3 partly compensates for the low pressures on the lower side of the wing. But the overall adverse pressure gradient due to the contraction still exists (the distance between two isobars indicates the pressure gradient). This pressure gradient causes the boundary layer on the fuselage below the wing to separate, as will be shown.

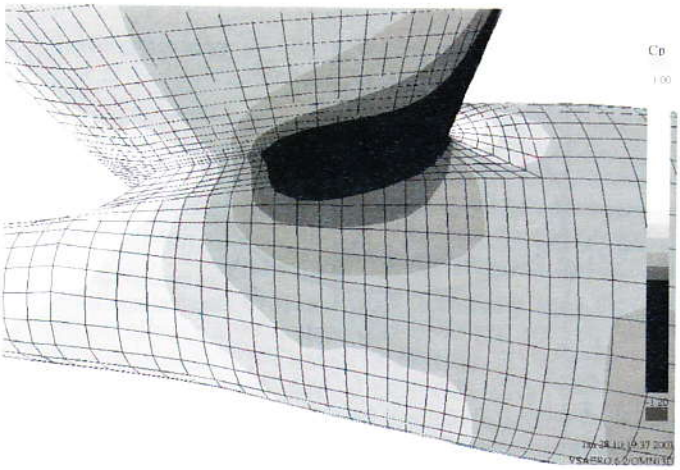

Figure 11. Invisc. C_p-distr.: model 1; CL=0.3, flap=0°.

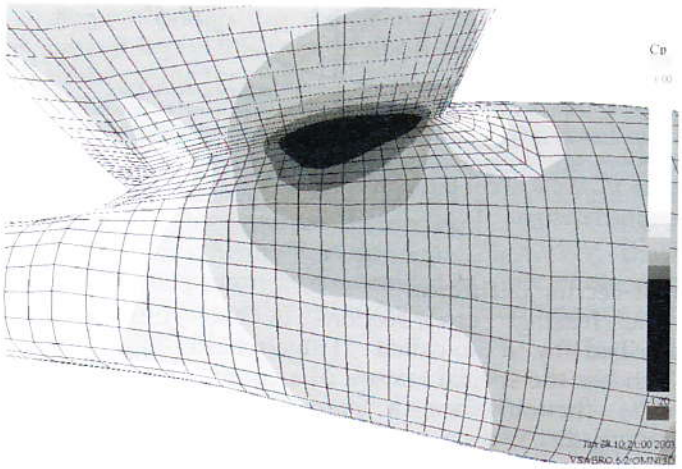

Figure 12. Invisc. C_p-distr.: model 3; CL=0.3, flap=0°.

One of the main tasks of the windtunnel measurements in 1998 (ref. 4) was flow visualization on wing and fuselage. The pictures taken during this investigation are compared to the results obtained from viscous calculations with VSAero. The viscous calculations, performed along streamlines that extend across all body panels, predict the three-dimensional transition-line of the flow. Restrictions exist with respect to flow separation; VSAero is not capable of calculating beyond separation, and stops the streamline development. Strictly speaking, the viscous calculation is quasi two-dimensional since the boundary layer development is calculated along each individual streamline.

Figure 13 shows a flow picture for model 1, taken in the windtunnel, and Figure 14 shows the calculated results of VSAero. Both pictures visualize the flow at C_L=0.3 with a flap setting of 0° and Reynolds Number of 700,000. The flow is visualized with a technique where fluorescent oil is illuminated with ultra-violet light. The turbulent boundary layer has more friction than the laminar one and drags more oil away, which results in a distinctive transition line. The forces acting on the oil are gravitation as well as friction. When the friction goes to zero (separation), gravitation and the accumulation of oil can disturb the flow pattern.

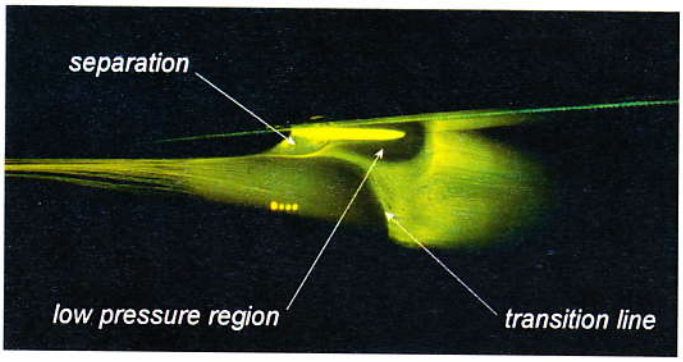

Figure 13. Model 1: windtunnel, Re=7E5, flap=0°.

In Figure 14 the calculated streamlines are colored according to the friction coefficient C_f, hence transition from laminar to turbulent flow is indicated by a sudden change of color. Separation is indicated by the ending of streamlines.

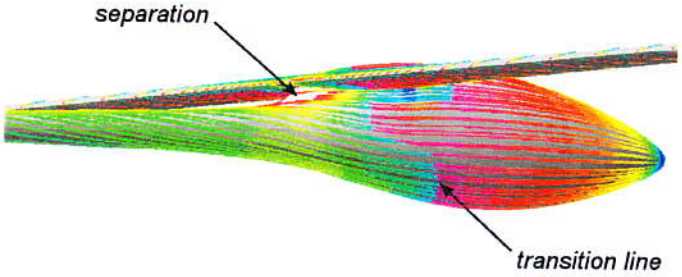

Figure 14. Model 1: calculation, Re=7E5, flap=0°.

When comparing the flow pattern from the windtunnel experiment with the calculated results, it becomes obvious that they correspond in many aspects: the positions of transition and separation are reasonably predicted by the calculation. Not shown is the horseshoe vortex around the wing root because the oil mixture used is not suited for this phenomenon. Likewise VSAero is not capable of calculating this vortex.

Design

Guidelines

With the experience from the preceding analysis, it is possible to set up a list of requirements for the design of a new wing- fuselage junction:

- Reduction of the contraction ratio and curvature of the fuselage below the wing
- Ninety-degree corner between lower wing surface and fuselage
- Optimal circulation distribution
- Wing-root airfoil suited for turbulent flow
- Maximum laminar flow area
- Prevention of separation
- Straight flap hinge line

- Gradually curved main spar
- Consideration of all flap deflections
- Application of wing-root fillets

The next sections explain the requirements in more detail and describe how they are implemented in a new design.

Contraction and curvature

The contraction of the fuselage below the wing causes a large local adverse pressure gradient. A horizontal cut through the configuration just below the wing is treated as an airfoil section, Figure 15. The contraction ratio depends on the width of the cockpit and the distance from the maximum width to the trailing edge of the pylon. Both moving the start of the contraction further upstream and the trailing edge downstream lower the pressure gradient in the wing-fuselage region. In addition, the curvature in this region has to be reduced to allow a gradual pressure recovery. Figure 15 shows the pressure distribution of the initial and an improved pylon shape.

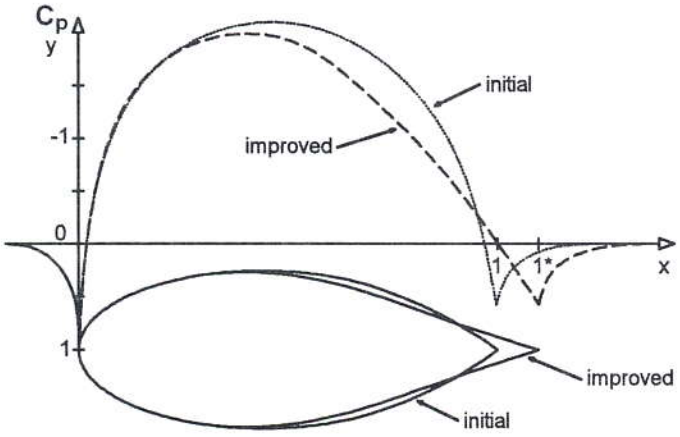

Figure 15. Horizontal cut through the fuselage below wing: initial and improved design.

Diffuser effect

In a vertical cut, the mutual influence of the lower side of the wing and the fuselage contour can be seen, Figure 16.

In the initial configuration the leading edge of the wing, in combination with the fuselage, form a nozzle, which is responsible for the pressure peak just behind the stagnation point of the wing. Aft of this point the fuselage contour and the lower side of the wing are shaped like a diffuser, resulting in a pressure distribution with a steep adverse gradient. In the improved design, the intersection lines of the fuselage and the lower side of the wing have the same direction of curvature. A positive wing twist opens the nozzle, which lowers the pressure peak at the nose.

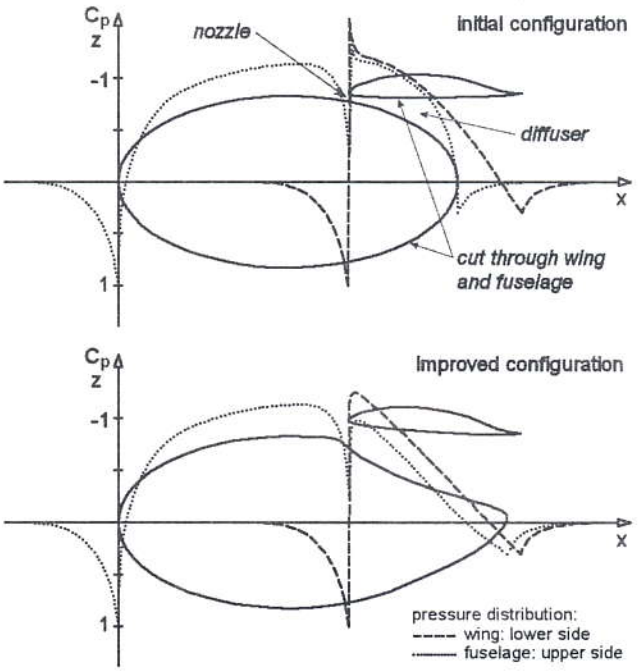

Figure 16. Vertical cut through wing and fuselage: initial and improved design.

Cross-section definition

The fuselage cross-sections of the ASW-27 are described by a so-called "Hügelschäffer-Egg-Curve" which has the special feature of a continuous curvature on its circumference, a prerequisite for a smooth pressure distribution and undisturbed boundary layer development. Its mathematical description only requires the coordinates of the upper (ZU) and lower (ZL) point in the plane of symmetry and the side-point at maximal width (YS, ZS). The coordinates (YP, ZP) for the egg-shaped cross-section can be constructed graphically as shown in Figure 17, or calculated with Eq. (2.1) to (2.3). Assuming θ, ZP follows from Eg. (2.1) and via ω in Eq. (2.2), YP follows from Eq. (2.3).

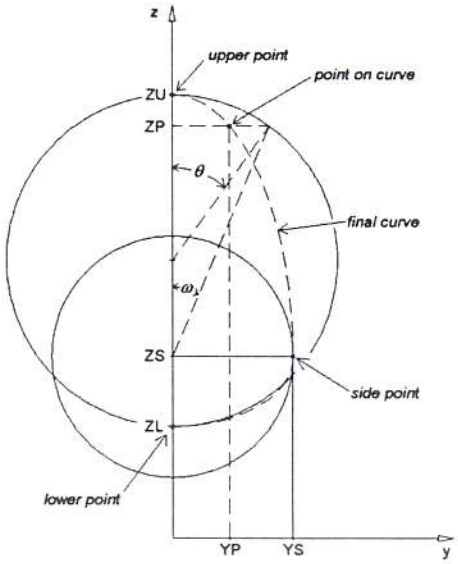

Figure 17. Hügelschäffer-Egg-Curve.

$$ZP = \frac{1}{2}\cdot(ZU + ZL) + \frac{1}{2}\cdot(ZU - ZL)\cdot\cos\theta \quad (2.1)$$

$$\omega = \arctan\left[\frac{1}{2}\cdot(ZU - ZL)\cdot\frac{\sin\theta}{(ZP - ZS)}\right] \quad (2.2)$$

$$YP = YS\cdot\sin\omega \quad (2.3)$$

An extended cross-section definition was developed which allows a 90 degree corner at the intersection with the wing (ref. 13), Figure 18 middle. It consists of three parts, where two are described with the previous relations plus an additional cosine-function in between. The cosine starts at the point of maximal width (YS, ZS) and extends to the point (YE, ZE), marking the intersection with the wing. Setting the end point of the cosine to (0, ZE), the function can also describe a sharp curve necessary for the pylon, Figure 18 right. In this case, it is possible to prescribe a tangent at the end point of the cosine function.

At the points where the cosine curve and the upper and lower egg-curve meet each other, the function has a continuous first derivative i.e. a vertical tangent. Since the second derivative, the curvature, is discontinuous, a wiggle in the pressure distribution could be expected. Calculations with VSAero show, however, that the present definition is convenient as only some discrete points of the curves are used for describing the surface to be panelled.

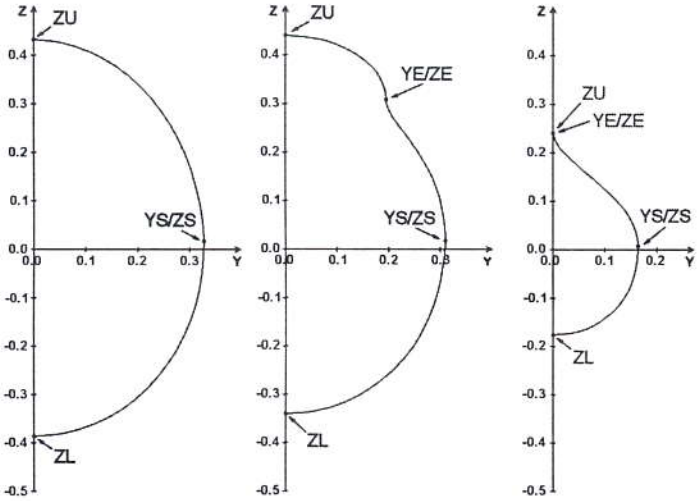

Figure 18. Section definition: egg-curve (left), extended curve (middle and right).

Wing twist

For the optimal circulation distribution that generates the lowest induced drag possible, the complete sailplane configuration should have an elliptical circulation distribution as formulated by Max Munk´s "stagger-theorem" (ref. 14). In this research the horizontal tailplane is neglected, as its lift contribution is positive or negative, depending on the center of gravity location, and small compared to that of the wing. The winglets were also neglected because they do not influence the circulation at the wing-fuselage section. The elliptical circulation distribution can be obtained by the application of wing twist. Since the flap hinge line must be straight, twist has to be applied around the flap hinge axis at 86% chord, which leads to a curved spar located at 40% chord. In order to reduce structural difficulties, the curvature of the spar needs to be small, i.e. large radii (ref. 15).

Airfoils

Special attention has to be paid to the boundary- layer development in the wing-root area. As described earlier, a turbulent wedge with origin at the wing root leading edge is present at low angles at attack. Windtunnel experiments show that the wedge angle behind an individual disturbance is approximately 15°; hence turbulence will spread with an angle of about 7.5° with respect to the direction of the streamlines (Figure 19).

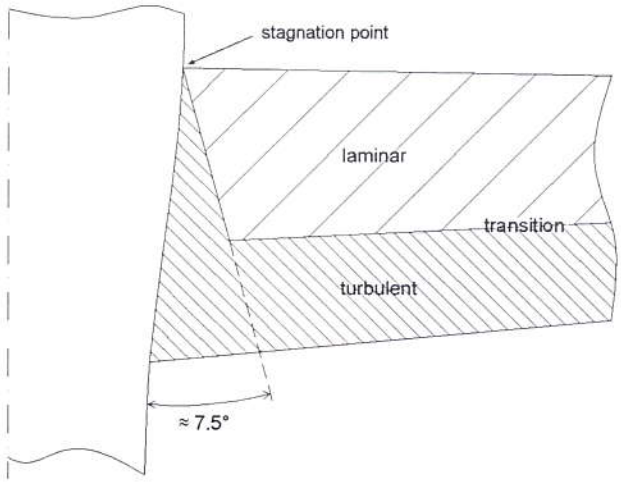

Figure 19. Turbulent wedge.

In turbulent flow, a "laminar" airfoil is usually inferior to a "turbulent" one. The latter type of airfoil has the position of minimum pressure (and maximum thickness) more forward compared to a laminar airfoil, which results in a smaller overall adverse pressure gradient. These effects are illustrated in Figure 20 and Figure 21, showing the basic airfoil DU89-134/14 and the modified DU89-134/14Root6, having an upper surface designed for laminar and for turbulent flow respectively. The pressure distribution is plotted for complete turbulent flow as well as for the corresponding inviscid flow (dotted line). Separation is present on the flap upper surface of the laminar airfoil and not on the turbulent one. From the turbulent airfoil applied in the wing center section up to 0.2 meter span, the wing is lofted to the laminar airfoil at 0.4 meter span.

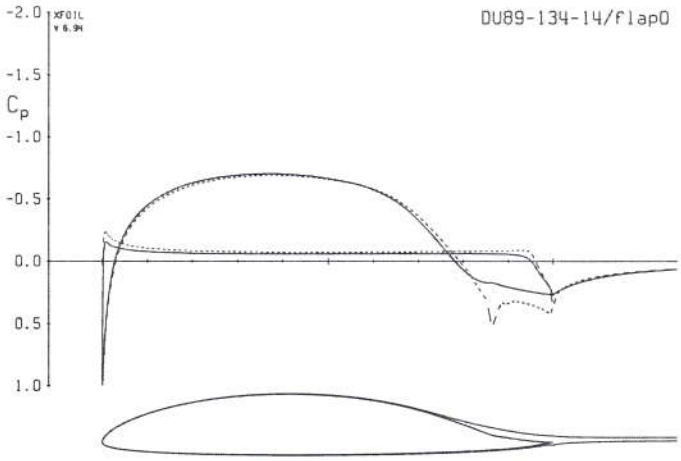

Figure 20. Turbulent Cp-distribution of laminar airfoil section DU89-134/14.

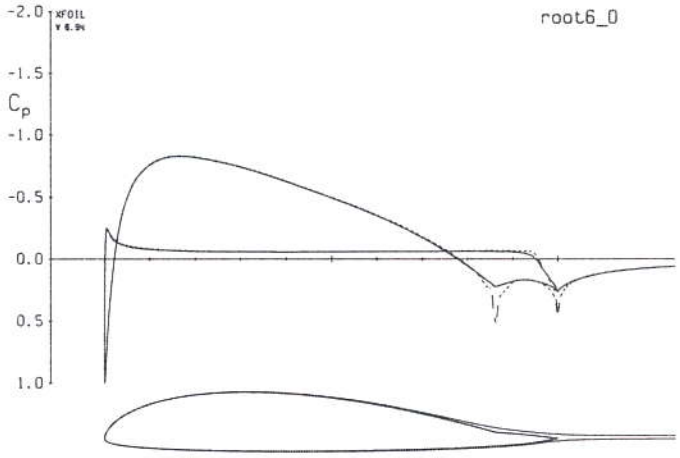

Figure 21. Turbulent Cp-distribution of turbulent airfoil section DU89-134/14Root6.

Rigid center-part airfoil

The main airfoil DU-89-134/14 was measured in the windtunnel up to a positive flap setting of 50°. This flap setting will be used in combination with neutral ailerons as a landing configuration. The result is a high-drag configuration that allows steep approaches and reduces the wing-root bending moments. Because of the extended fuselage pylon, it is not possible to deflect a continuous flap to 50°. For structural simplicity the wing will have a small rigid center-part on top of the pylon. The spanwise extend of the rigid part is chosen such that the flap can deflect freely, without touching the pylon. Since the best glide ratio occurs at a flap deflection of 12.5° the flap is continuous with the rigid center-part at this position. The gap between the rigid part and the flap will be sealed by vertical fences in order to prevent cross flow.

Fillets

In the final geometry, quarter-circular fillets at the wing-fuselage intersection are necessary. These fillets extend from the leading edge to the trailing edge with increasing radius. They mainly fulfil two tasks: carefully shaped they can reduce the venturi- and diffuser effect in the wing-root area. They also round off the sharp 90° corner of the intersection, which avoids the formation of longitudinal vortices. These fillets are not included in the present geometries since VSAero is not capable taking the effect into account.

Geometry

All the aspects described before have been implemented in the new wing-fuselage design in an iterative process with many changes necessary to achieve the optimal result, named Version 4996.

Figure 22ba, -b and -c present the geometry of Version 4996. Note that the final geometry does not include wing-dihedral, since its main task is the preparation of a windtunnel model.

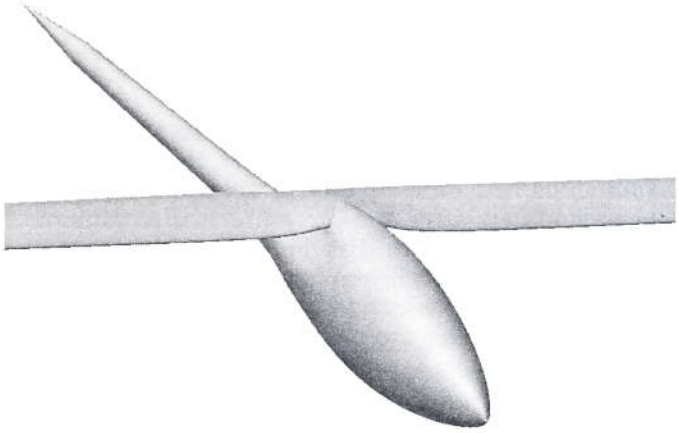

Figure 22a. Version 4996, front-isometric view.

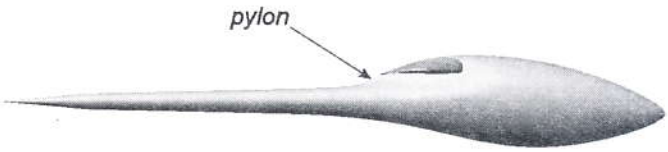

Figure 22b. Version 4996, no wing-dihedral, side view.

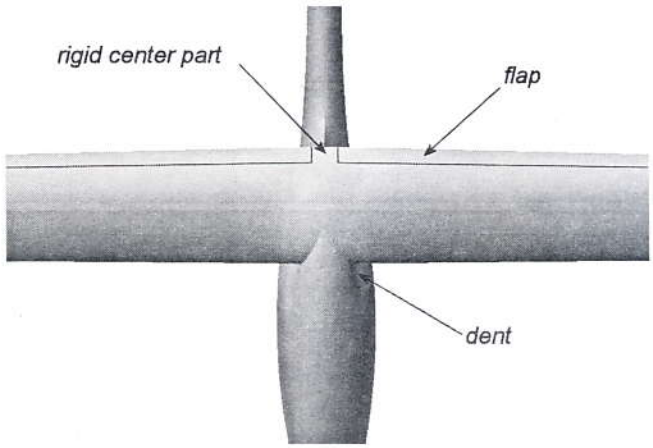

Figure 22c. Version 4996, top view.

Inviscid calculations

The geometry of Version 4996 is calculated for the range of lift coefficients from C_L=0.3 to C_L=1.2. Figure 23 shows the circulation distributions, the wing twist applied, and the k-factors for the key lift coefficients and corresponding flap deflections. The results can be compared to those of Models 1 and 3 in Figure 8.

The center section of the wing has a positive twist of 7.15° with respect to the untwisted part beyond 2.0 meter span, set at an incidence of -0.65°. At a flap deflection of 12.5°, the flap and the rigid airfoil section in the center are continuous and at the corresponding C_L=0.7, the circulation distribution is a smooth curve up to the position where the wing intersects the fuselage. Here the circulation slightly drops. It is impractical to further increase the twist in this region because only the upper side of the wing can contribute to the circulation, and the lower side is within the fuselage. For all other flap settings, the rigid center-part causes only a small change in the circulation distribution as well and the effect on the k-factor is consequently negligible. As a result, all circulation distributions are close to the elliptical one at the same lift coefficient.

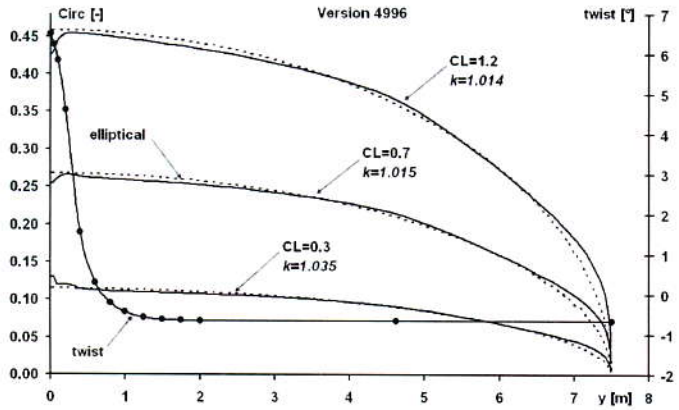

Figure 23. Circulation distributions and k-factors: Version 4996.

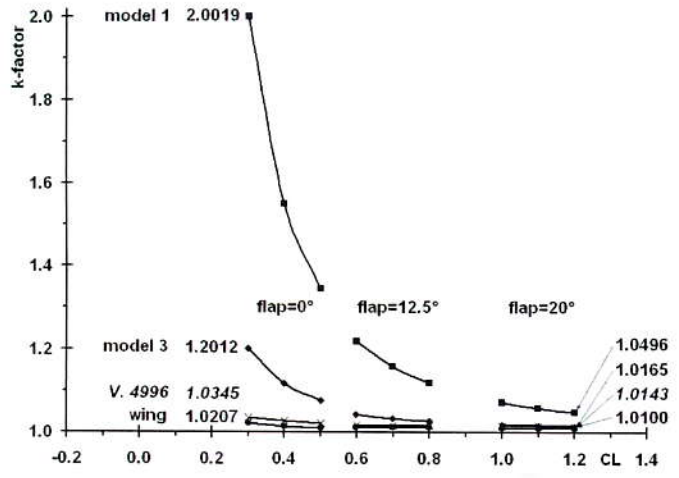

Figure 24. k-factors: Version 4996, model 1, model 2 and wing.

The performance of Version 4996 is shown in Figure 24, which is the same plot as Figure 9 used in the analysis. In comparison with Models 1 and 3, the induced drag of Version 4996 has improved substantially at the lower lift coefficients. The k-factors of Version 4996 are close to the k-factors of the wing only. Comparing Version 4996 to Model 3 at a flap setting of 0° and C_L=0.3, the k-factor is reduced from 1.2012 to 1.0345, i.e., a reduction of 16.5%. With a wing loading of $365^{N}/_{m^2}$, C_L=0.3 corresponds to a flight speed of $160^{km}/_{h}$. Assuming that the induced drag contribution is $^{1}/_{3^{rd}}$ of the total drag at this lift coefficient, a reduction of 16.5% of induced drag would lead to 5.5% less total drag, hence a 5.5% lower sink rate.

Viscous calculations

The viscous flow calculations show the position of transition and separation on the wing and fuselage. The upper side of the wing is interesting at low flight speed when C_L=1.2, Re=1,000,000, and the flap deflection is 20°. This condition is shown in Figure 25. The lower side of the wing is critical at the lower end of the drag bucket. Therefore C_L=0.3, Re=2,000,000, and a flap deflection of 0° is relevant, Figure 26.

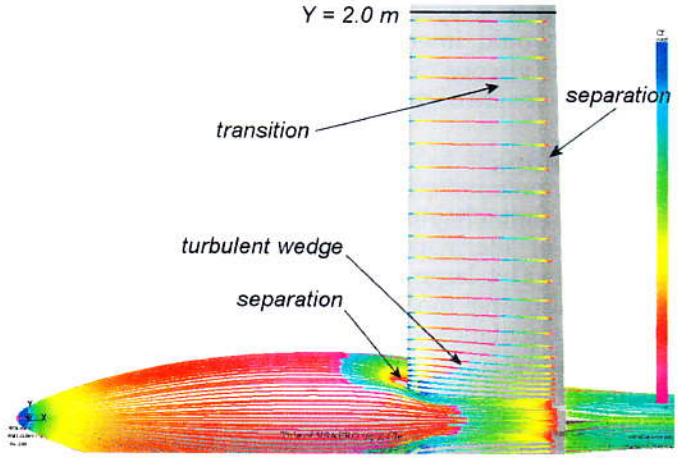

Figure 25. Visc. calc.: Version 4996, upper side, flap 20°, Re=1E6, CL=1.2.

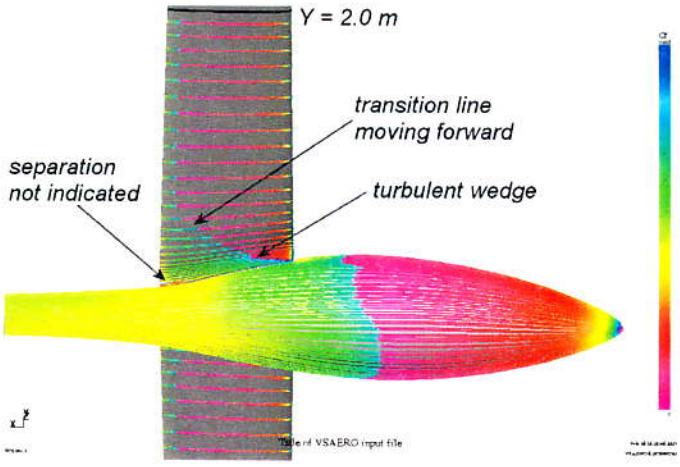

Figure 26. Visc. calc.: Version 4996, lower side, flap 0°, Re=2E6, CL=0.3.

As mentioned earlier, VSAero is not capable of calculating the horseshoe vortex in the wing-fuselage juncture and the turbulent wedge on the wing-root. Therefore, this wedge was artificially made by tripping the boundary layer on certain panels.

On the upper side of the wing the laminar boundary layer extends, without any change in chordwise direction, up to a position very close to the fuselage. The transition line of the wing intersects the turbulent wedge at a spanwise position of 0.4 meter, where the laminar airfoil is present. Note that the program indicates separation in front of the trailing edge on the flap. Due to the limited number of iterations used, the program has not taken the effect of the boundary layer on the pressure distribution fully into account. Both experiments and converged two-dimensional calculations show that separation does not exist there. It is important that no additional separation is predicted at the center section. Due to the stagnation point, the calculation indicates separation in front of the wing-root leading edge. This can be eliminated by applying a wing leading edge fairing (ref. 16).

The lower surface also shows that the transition line is straight up to a spanwise position of 0.55 meter, just before it would intersect the turbulent wedge (at 0.4 meter). The viscous calculation does not show separation on the lower side of the wing or fuselage.

Conclusions

In the first chapter of this paper, the unexpected outcome of the windtunnel measurements has been explained. The large differences in drag between the three windtunnel models can be primarily addressed to different circulation distributions, resulting in different induced drag contributions. It has been shown that the boundary layer on the wing-fuselage juncture is also highly influenced by interference effects creating areas of separation especially on the pylon.

With an iterative integral design process taking inviscid- and viscous flow into consideration, it is possible to reduce the interference problems. A combination of changing fuselage sections, wing sections and, in particular, wing twist, led to a substantial reduction in induced drag: the final design has an almost elliptical circulation distribution and corresponding minimum induced drag. Viscous flow calculations indicate that separation on the fuselage-pylon or the upper- and lower wing side at the juncture will not occur. The actual drag reduction, however, need to be verified by future windtunnel tests and compared to previous results (ref. 8).

References

1. L.M.M. Boermans, K. Kubrynski, F. Nicolosi: Wing-fuselage design of high-performance sailplanes. Proceedings of the Seminar "Boundary-Layer Separation in Aircraft Aerodynamics", Delft University Press, 1997.
2. H. Schlichting, E. Truckenbrodt: Aerodynamik des Flugzeugs. Zweiter Band, Berlin-Göttingen-Heidelberg, Springer Verlag, 1960.
3. F. Thomas: Fundamentals of sailplane design. College Park Press, College Park, Maryland, 1999.
4. D. Kaspari: Windkanaluntersuchungen an drei Flügel-Rumpf-Kombinationen der Akaflieg München am Low Speed Aerodynamics Laboratory der TU-Delft. Semesterarbeit, Fachhochschule München, 1998.
5. H. Nithianandrajah: Windtunnel tests of three wing-fuselage combinations and the mechanical actuation of the angle of attack for models spanning the tunnel. Final year project, February-June 2002, TU-Delft, Imperial College.
6. L.M.M. Boermans, A. van Garrel: Design and windtunnel test results of a flapped laminar flow airfoil for high-performance sailplane applications. Technical Soaring vol. XXI, No 1, 1997.
7. R. Phillip: Untersuchung eines Flügel-Rumpf-Übergangs für ein Segelflugzeug mit Hilfe eines Panelverfahrens. Semesterarbeit, at TU-Delft, Faculty of Aerospace Engineering, for the Technische Universität München, Lehrstuhl für Fluidmechanik, 1997.
8. L.M.M. Boermans: D.C. Terleth: Windtunnel tests of eight sailplane wing- fuselage combinations. Technical Soaring vol. VIII, No 3, 1984.
9. J. K. Nathman: VSAero, a computer program for calculating the nonlinear aerodynamic characteristics of arbitrary configurations. Users Manual, version 6.2, 2001.
10. R. Berger: Konstruktion der Oberflächengeometrie eines Segelflugzeugs und aerodynamische Untersuchung mit einem Panelverfahren. Technische Universität München, LT-SA 02/09, 2002.
11. M. Drela: XFoil 6.9 User Guide. MIT Aero & Astro Harold Youngren, Aerocraft Inc., January 2001.
12. R. Berger: Entwicklung eines Lastannahmen Tools, beispielhafte Anwendung auf das Segelflugzeug Mü-31. Akaflieg München, Lehrstuhl für Luftfahrttechnik, September 2001.
13. E. N. Jacobs, K. E. Ward: Interference of wing and fuselage from tests of 209 combinations in the NACA variably density tunnel. NACA-Report No. 540, 1936.
14. M. Munk: The minimum induced drag of aerofoils. NACA-Report No. 121, 1921.
15. A. Seitz: Auslegung und Konstruktion des Tragflächenmittelstücks eines FAI 15m Rennklasse Segelflugzeugs. Akaflieg München, Lehrstuhl für Leichtbau, Januar 2002.
16. C.B. Steenart, B.W. van Oudheusden, L.M.M. Boermans: Simplified design method for a symmetrical wing-body fairing. 23nd ICAS Congress, paper 2.9.4, 2002.